INTERNATIONAL JOURNAL OF PRECISION ENGINEERING AND MANUFACTURING-GREEN TECHNOLOGY Vol. 3, No. 4, pp. 359-365 OCTOBER 2016 / 359
DOI: 10.1007/s40684-016-0045-z ISSN 2288-6206 (Print) / ISSN 2198-0810 (Online)

Comparative Study on Mechanical Properties of CR340/CFRP Composites through Three Point Bending Test by Using Theoretical and Experimental Methods

Min Sik Lee[1], Hyung Yoon Seo[2], and Chung Gil Kang[3,#]

1 Department of Mechanical Engineering, Pusan National University, 2, Busandaehak-ro 63beon-gil, Geumjeong-gu, Busan, 46241, South Korea
2 Department of Electrical and Computer Engineering, Pusan National University, 2, Busandaehak-ro 63beon-gil, Geumjeong-gu, Busan, 46241, South Korea
3 School of Mechanical Engineering, Pusan National University, 2, Busandaehak-ro 63beon-gil, Geumjeong-gu, Busan, 46241, South Korea
Corresponding Author / Email: cgkang@pusan.ac.kr, TEL: +82-51-510-1455, FAX: +82-51-518-1456

KEYWORDS: Simulation, Three-Point bending test, Hashin damage, Forming limit diagram, Carbon fiber reinforced plastic (CFRP)

In this study, Cold Rolled 340 (CR340)/Carbon Fiber Reinforced Plastic (CFRP) composites were fabricated, and experiments and simulation were performed to compare their flexural properties from three-point bending tests. The mechanical properties of CR340 and CFRP were input by dividing the material regime into elastic, plastic, and fracture regions in order to improve the simulation reliability. A forming limit diagram was determined through a stretch test for the CR340 steel plate and used as data input in the simulation. For CFRP, simulation was carried out using the Hashin damage theory and damage evolution obtained from references. Results showed that the maximum bending stress, fracture displacement, and gradient in the experiments closely matched those obtained from the simulation.

Manuscript received: July 14, 2016 / Revised: September 18, 2016 / Accepted: September 20, 2016
This paper was presented at ISGMA2016

1. Introduction

In the automobile industry, there has been an increasing focus on developing environmentally friendly materials for improved safety, reduced weight, higher fuel efficiency, and lower environmental contamination. Furthermore, with the increasing demand for higher performance and efficiency, the low weight of vehicles is not an option but is mandatory.[1,2]

With increasingly stringent environmental regulations, automobile manufacturers worldwide are focused on developing environmentally friendly automobiles by employing biotechnology, natural fuels, and hybrid, electric, and fuel cell vehicles. However, hybrid vehicles require additional battery and electric devices that increase their weight by around 100 kg, while fuel cell vehicles contain additional equipment that increases their weight by around 200 - 250 kg. One of the key approaches to increasing the fuel efficiency of environmentally friendly automobiles is to make the vehicles lightweight. The development of lightweight vehicles is currently limited to only implementation of high strength steel, hot press, and TWB technology. Therefore, for the future development of such automobiles, materials lighter than steel with specific strength and stiffness should be used.

Accordingly, as next-generation materials such as high strength aluminum alloy, magnesium, and fiber-reinforced composites are developed, they are also being implemented in automobiles parts. Among such materials, carbon fiber reinforced plastic (CFRP), which is a fiber-reinforced composite, has excellent specific strength and specific stiffness, and therefore, it has been studied extensively.[3,4] However, there are limitations in using CFRP as automobiles parts during collisions, owing to the low elongation rate and low fracture toughness of CFRP. To resolve these problems, studies on hybrid composite materials are focusing on overcoming these limits by bonding CFRP with metals.[5]

Teng et al.[6] studied the fracture mode of CFRP with respect to its bonding characteristics with a metal structure reinforced with CFRP. Narmashiri et al.[7] studied the effect of a bonded CFRP plate in an i-beam on the increase in the bending load and strain restriction, and the effect of the CFRP ratio on the shear strain rate. El-Tawil et al.[8] showed that a metal hinge wrapped with CFRP was good for low-frequency fatigue behavior, restricted partial buckling, and delayed distortion. Hankeln and Mahnken[9] evaluated the formability of unidirectional single material CFRP through simulations. They designed CFRP by dividing it into reinforcement materials and matrix, and studied the

© KSPE and Springer 2016

Table 1 CFRP properties

Type	Resin content (%)	Resin viscosity (cps at 25 °C)	Fabric thickness (mm)
Plain	35	140	0.25

Table 2 CR320 properties

Tensile strength (MPa)	Elongation (%)	Vickers hardness (Hv)	Elastic modulus (GPa)
496	27	140	210

effect of the anisotropy of CFRP on the strain behavior according to viscosity and temperature. However, unidirectional CFRP exhibited anisotropic strain behavior and was determined to be unsuitable for automobiles parts, which are required to cope with collision in several directions. Furthermore, the incorporation of CFRP materials in automobiles by only using experimental methods may be expensive and time-consuming. Currently, CAE technology through finite elements for various metal materials is widely used. Although CAE technology has been proved reliable, its use for the anisotropic materials such as CFRP and composite materials is limited, and its reliability for such materials has not yet been confirmed. Further, the changes in the mechanical properties of the final material in CFRP and metal hybrids need to be investigated.

In this study, CR340, which has an excellent elongation rate, was stacked with CFRP as a reinforcement material for automobiles, and experiments and simulation were performed for comparison through three-point bending tests. The mechanical properties of CR340 and CFRP are input by dividing the material into elastic, plasticizer, and fracture regions in order to improve the simulation reliability. Furthermore, the simulation reliability was ensured by comparing the simulation and experiment data.

2. Experiment and Simulation

2.1 Experiment

2.1.1 Materials

A plain woven carbon fiber from Toray was used as the CFRP material in the present experiment. The thickness of one prepreg sheet was 0.25 mm, and a thermosetting resin with an initial epoxy weight percentage of 35% was used. The physical properties of CFRP are presented in Table 1.

In this study, instead of using a high strength steel plate such as DP steel or boron steel, CFRP was stacked on the CR340 steel plate to increase the specific strength, specific stiffness, and fracture toughness. The thickness of the CR340 steel plate was 0.9 mm. Its mechanical properties are presented in Table 2.

2.1.2 Stretch Test for FLD Curve

The steel used in the stretch test was CR340. Fig. 1 shows the stretch test specimens and ARAMIS data measured via a three-dimensional (3D) coordinate measuring machine after stretch tests. The stretch test was performed just before fracture occurred in each test

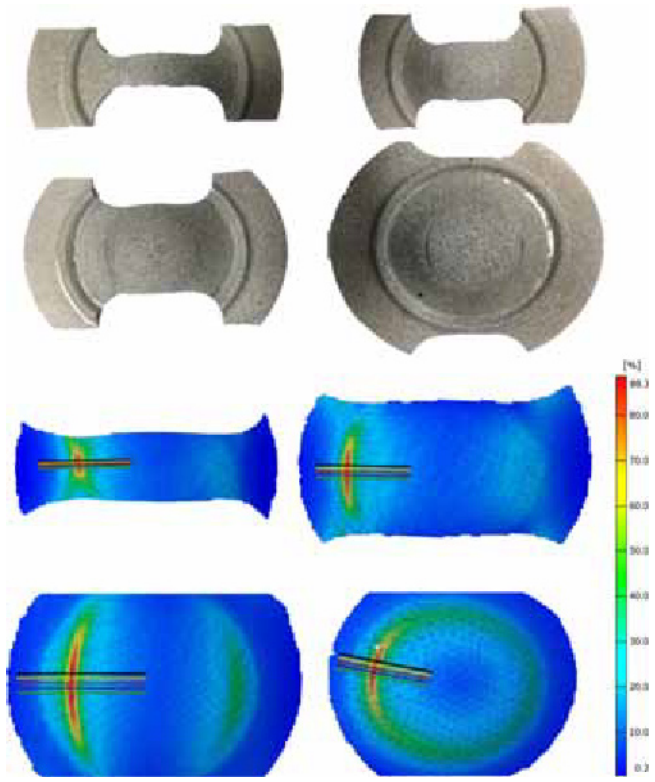

Fig. 1 Stretch test and 3D measurement for FLD curve

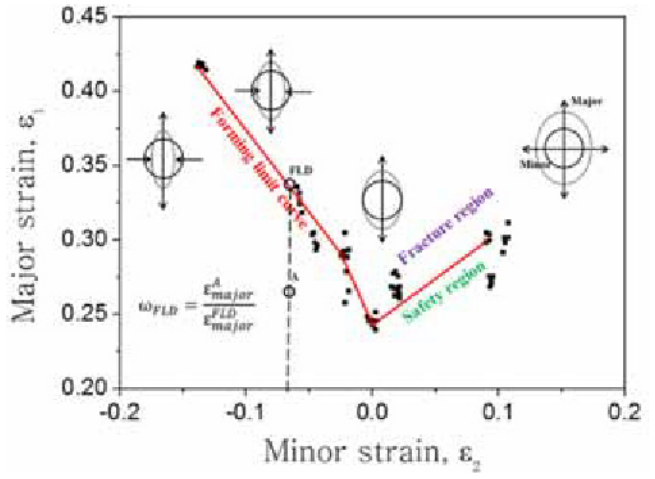

Fig. 2 FLD curve of CR340

Table 3 FLD condition

Punch load (kN)	Punch velocity (mm/s)	Lubricant condition	Software for strain measurement	Load for detecting fracture (kN)
500	1	NO	ARAMIS	0.1

specimen. The details of the forming limit diagram (FLD) testing conditions are outlined in Table 3. The test was conducted under lubrication-free conditions, and the fracture sensing load was 0.01 ton. Major and minor strains were obtained with the fractured test specimens using ARAMIS, and a fracture mechanism was applied. Fig. 2 shows the FLD curve obtained after the stretch test. Minor and major

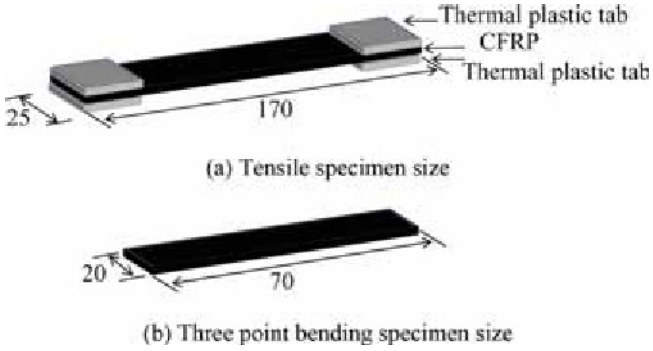

Fig. 3 Specimen size for tensile and three-point bending test

strain data were applied in the simulation, and the damage evolution value was defined at 0.1 mm as a fracture value.

2.1.3 Tensile Test and Three-Point Bending Test

Fig. 3 shows the experimental apparatus and specimen size for the tensile and bending tests. The size of the test specimen for the three-point bending test was 70 × 20 mm and the length of span (L) was 42 mm, as per the specifications in ASTM (D790-03). Three-point bending was executed with a punch speed at 10 mm/min. The specimen size for the tensile test was 170 × 25 mm. Thermal plastic tabs were attached to the end of the tensile specimens to prevent fracture along the grip line of the specimens during tensile test and the tensile test was conducted at a speed of 2 mm/min.

2.2 Simulation

2.2.1 Damage Initiation Criteria and Damage Evolution for CR420

The necking of metal causes unstable phenomena during metal formation. In particular, if local necking occurs in a thin plate, it can lead an abrupt fracture. Because the sheet metal in the simulation is very thin, local necking could not be realized in the shell element. In this study, forming limit curve data obtained through testing were applied to the simulation. The simulation then proceeded to predict the onset of necking instability in the sheet metal using the FLD curve in Abaqus/explicit.

As shown in Fig. 2, the FLD damage initiation criterion was met when $W_{FLD} = 1$, where the variable W_{FLD} is a function of the current deformation state. W_{FLD} was defined by following equation:

$$W_{\mathrm{FLD}} = \varepsilon_{\mathrm{major}} / \varepsilon_{\mathrm{major}}^{\mathrm{FLD}} \tag{1}$$

where $\varepsilon_{\mathrm{major}}$ is the current major principal strain, and $\varepsilon_{\mathrm{major}}^{\mathrm{FLD}}$ is the measured principal limit strain, which is the boundary of the forming limit curve. For example, if, when the sheet was formed, $\varepsilon_{\mathrm{major}}$ of one element increased by $\varepsilon_{\mathrm{major}}^{\mathrm{FLD}}$, damage initiation occurred, as shown in Fig. 2.

FLDs basically rely on the changes in the strain path, and if the strain path is linear, the performance is good. However, if the strain path is nonlinear, FLDs should be used carefully. An FLD curve with a linear strain path can be seen in Fig. 2. The FLD curve is generally affected by temperature or field variables, but the bending test in this study was conducted at room temperature. Thus, it was sufficient to use the single FLD curve that was obtained at room temperature.

In the case of a shell element, for which only a plane stress formulation is used, necking should be interpreted along with the damage evolution. Once the material reaches the damage initiation criterion, an effective plastic displacement, at the timing defined in the evolution equation, can be obtained. Effective plastic displacement can be measured with the following equation:

$$\dot{\bar{u}}^{pl} = L\dot{\bar{\varepsilon}}^{pl} \tag{2}$$

where L is the length of an element, and $\dot{\bar{\varepsilon}}^{pl}$ is the speed of the effective strain. Once the effective plastic displacement reaches the fracture displacement, fracture occurs immediately. Damage evolution is linear, and the damage variable is increased according to the following equation:[10]

$$\dot{d} = \frac{L\dot{\bar{\varepsilon}}^{pl}}{\bar{u}_f^{pl}} = \frac{\dot{\bar{u}}^{pl}}{\bar{u}_f^{pl}} \tag{3}$$

When the material reaches the damage evolution, its strength is degraded. The effective plastic displacement ($\bar{u}_f^{pl}$) of damage evolution used in this paper was set at 0.15 mm.

2.2.2 Damage Initiation Criteria and Damage Evolution for CFRP

Hashin's criteria theory was used as the damage initiation criteria for the CFRP. This theory states that damage is initiated when one of the four values of fiber tension (F_f^t), fiber compression (F_f^c), matrix tension (F_m^t), or matrix compression (F_m^c) reach the fracture strength of the CFRP. Details are given below.[11,12]

Fiber tenstion ($\sigma_{11} \geq 0$)

$$F_f^t = \left(\frac{\sigma_{11}}{x^T}\right)^2 + \left(\frac{\tau_{12}}{S^L}\right)^2 \tag{4}$$

Fiber compression ($\sigma_{11} < 0$)

$$F_t^c = \left(\frac{\sigma_{11}}{x^C}\right)^2 \tag{5}$$

Matrix tension ($\sigma_{22} \geq 0$)

$$F_M^t = \left(\frac{\sigma_{22}}{\gamma^T}\right)^2 + \left(\frac{\tau_{12}}{S^L}\right)^2 \tag{6}$$

Matrix compression ($\sigma_{22} < 0$)

$$F_M^C = \left(\frac{\sigma_{22}}{2S^T}\right)^2 + \left[\left(\frac{\gamma^C}{2S^T}\right)^2 - 1\right]\frac{\sigma_{22}}{\gamma^C} + \left(\frac{\tau_{12}}{S^L}\right)^2 \tag{7}$$

where σ_{ij} are the elements of each stress tensor, while X^T and X^C are the tensile strength and compressive strength of the fiber, respectively. Y^T and Y^C are the tensile strength and compressive strength of each matrix, respectively. S^L and S^T are the longitudinal and transverse shear strength, respectively.

σ_{11}, σ_{12}, and τ_{12} are the components of the effective stress tensor, σ_{ij}, that is used to evaluate the initiation criteria, and is computed by:

Table 4 Elastic modulus of CFRP[16,17]

Density (g/cm^3)	Elastic modulus (GPa)					
	E1	E2	Poisson's ratio	G12	G13	G23
1.7	130	8	0.32	4.5	4.5	3.5

Table 5 Strength and damage evolution of CFRP[17]

(MPa)	X^T	X^C	Y^T
CFRP	2000	2000	61
	Y^C	S^L	S^T
	130	85	40
G_{ft} (mJ/mm^2)	G_{fc}	G_{mt}	G_{mc}
91.6	79.9	5	5

$$\sigma_{ij} = M\sigma'' \tag{8}$$

where σ is the nominal stress, and M is the damage operator.[13,14]

$$M = \begin{bmatrix} \frac{1}{(1-d_f)} & 0 & 0 \\ 0 & \frac{1}{(1-d_m)} & 0 \\ 0 & 0 & \frac{1}{(1-d_s)} \end{bmatrix} \tag{9}$$

d_f, d_m, and d_s are internal (damage) variables that characterize fiber, matrix, and shear damage, respectively, and are derived from the damage variables d_f^t, d_f^c, d_m^t, and d_m^c, corresponding to the four modes previously discussed, as follows:[14]

$$\begin{aligned} d_f &= \begin{cases} d_f^t & if \quad \hat{\sigma}_{11} \geq 0, \\ d_f^c & if \quad \hat{\sigma}_{11} < 0, \end{cases} \\ d_m &= \begin{cases} d_m^t & if \quad \hat{\sigma}_{22} \geq 0, \\ d_m^c & if \quad \hat{\sigma}_{22} < 0, \end{cases} \\ d_s &= 1-(1-d_f^t)(1-d_f^c)(1-d_m^t)(1-d_m^c) \end{aligned} \tag{10}$$

Detailed data for each of Hashin's criteria regarding the fracture of a composite are given in Tables 4[15,16] and 5.[16]

2.2.3 Modeling for Shear and Bending Test

The ABAQUS/explicit software was used to perform the bending simulation. Fig. 4 shows the modeling of the three-point bending and stacking method in the simulation. The punch and supporting round were 5 mm, as shown in Fig. 4(a). The CFRP was stacked on CR340. The method of CFRP stacking is depicted in Fig. 4(b). Unidirectional fiber was provided as input data into ABAQUS. In the actual experiment, two CFRP sheets were crossly stacked at 0° and 90°, so that if five sheets of CFRP are stacked, the thickness would be 1.1 mm. In the simulation, CFRP sheets were laminated with an 11-ply laminar and were repeatedly stacked at 0° and 90°. Ten unidirectional CFRPs with a thickness 0.11 mm were stacked in order to provide the same thickness. The specimen mesh size was 1 mm and 0.5 mm was applied

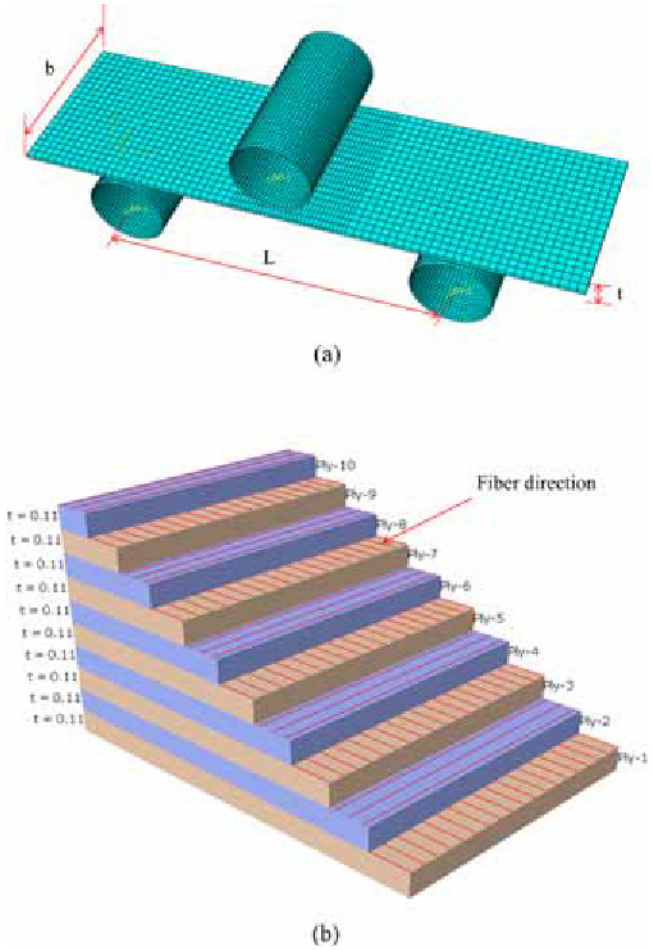

Fig. 4 Three-Point bending test and fiber orientation model

at bending point, as shown in Fig. 4(a).

Both CR340 and CFRP were SR4 shell elements and had thicknesses of 0.9 and 1.1 mm, respectively. By assuming that CR340 and CFRP are well bonded, a tie condition was used for contact condition between CR340 and CFRP. The materials were tied so that even if fracture occurred during three-point bending, they would not be delaminated. Further, since two specimens were bonded by epoxy, the interaction property condition was also considered to give the effect of cohesive behavior.

A friction coefficient of 0.1 was used, and the punch and supporting R were fixed and punch velocity was 10 mm/s to reduce the simulation time. Mass scaling was not used, and the stable time increment size was 4.80452 E-7 and the total cup time was 14400 s.

2.2.4 Input Data for Simulation

The physical properties data entered in the simulation are seen in Fig. 5. Zone a-b at location No. 1 is the elasticity zone, for which an elastic modulus value of 210 GPa was used, while the b-c zone at location No. 2 is a plasticity deformation zone, for which the S-S curve was entered based on the tensile strength test data for CR340. Zone c-d at position No. 3 is a fracture zone based on the tensile strength. The criterion for the gradient of stress to cause a lower response, as in zone c-d, is governed by damage initiation. If the damage theory is not applied, the fracture mechanism does not occur and stress responds as

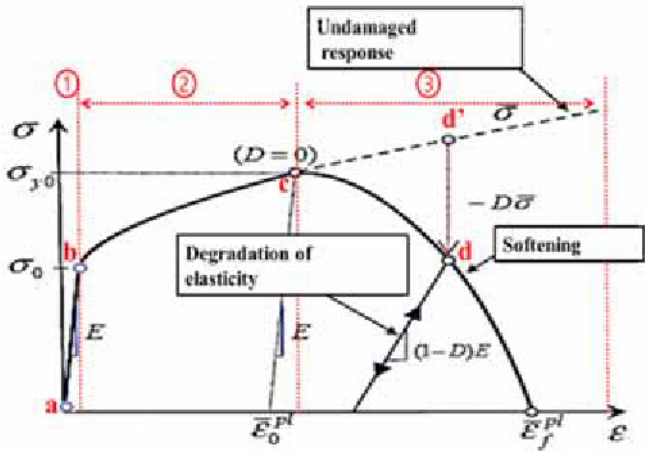

Fig. 5 Material input method with respect to region

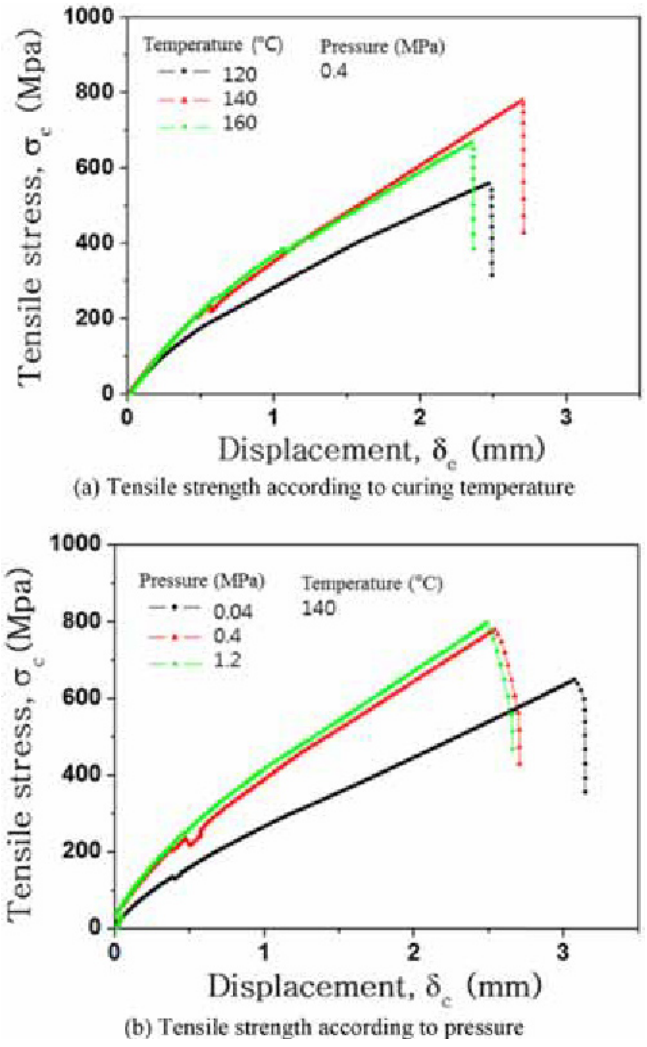

Fig. 6 Curve of tensile stress and displacement according to temperature and pressure

in zone c-d after necking. In other words, after the bending in the simulation, the material is elongated infinitely without fracture and stress is not decreased. In this study, the FLD for CR420, which was obtained earlier, was applied in order to obtain accurate data for the fracture mechanism. For the CFRP, the CFRP laminar was anisotropic

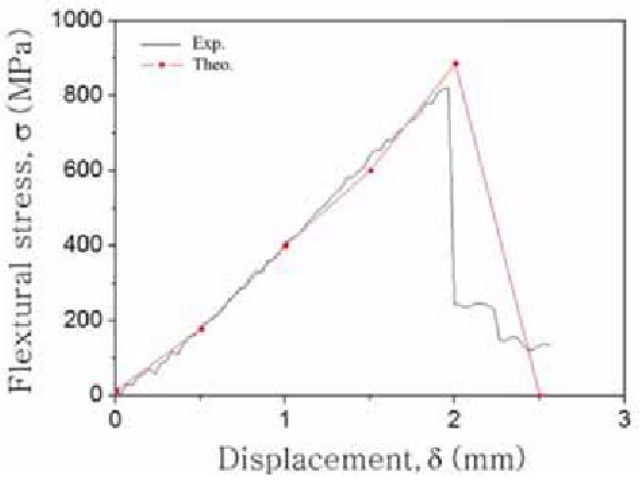

Fig. 7 Comparison of flexural stress of CFRP between experiment and simulation

material. The elastic modulus is listed in Table 4. The Hashin theory was applied for the damage initiation criteria. Detailed data for the strength and damage evolution are given in Table 5.

3. Results and Discussion

3.1 Tensile Test of CFRP according to Process Parameters

Fig. 6 shows the tensile strength of CFRP according to the curing temperature and pressure. Figs. 6(a) and 6(b) show that the tensile strength was highest at a temperature and pressure of 140 °C and 0.4 MPa, respectively, and therefore, these conditions were used for producing the test specimens. During specimen production, although the tensile test was favorable for specimens produced at pressure under 1.2 MPa, the epoxy spilled out and spread on the die. Consequently, the specimen thickness decreased, and despite the high tensile strength, the loss of epoxy resulted in a decrease in the interfacial strength between the CFRP laminate.

3.2 Three-Point Bending of CFRP and CFRP/CR340 Composite

The three-point bending test specimen was fabricated at 140 °C and 0.4 MPa, according to the results of the tensile test shown in Fig. 6. Fig. 7 shows a comparison between the experimental and simulation data after bending test for five sheets of CFRP fabric. With elastic modulus and Hashin damage theories applied in the simulation, simulation results shared distinct similarities with the testing result. Fracture occurred at 2 mm, which was almost similar at all the points, while the gradient and fracture strength were also similar to the testing results.

Fig. 8 shows a comparison of the experiment and simulation of three-point bending test results for CFRP/CR340 composite. The bending strength in the experiment for the CFRP/CR340 composite was 711 MPa, while it was 755 MPa in the simulation, both of which did not show a large error. The gradient also showed similar results. This similarity could be attributed to the selection of the input elastic modulus region, plastic region, and fracture region in detail while entering data for simulation, as shown in Fig. 5.

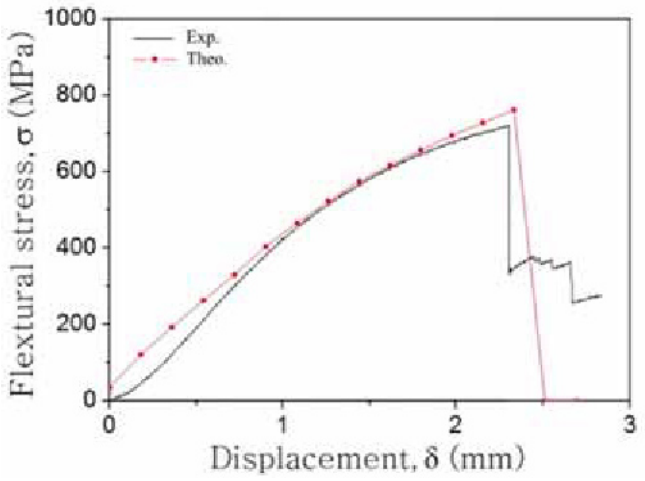

Fig. 8 Comparison of flexural stress of CR340/CFRP between experiment and simulation

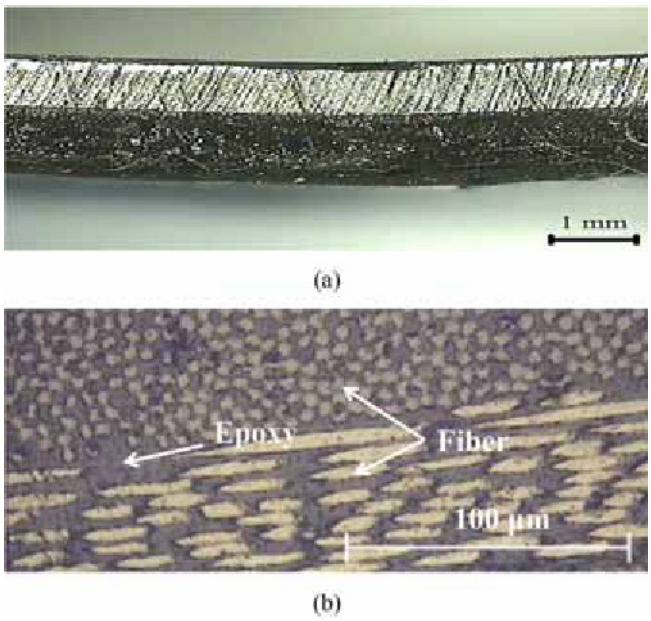

Fig. 9 Specimen after bending test and microstructure of CR340/CFRP composites

In this experiment, the bonding condition, which is a constraint condition between CR340 and CFRP composite materials, was a tie. If this contact condition is investigated closely and the delamination during shear stress and fracture by epoxy is studied, better results could be obtained.

3.3 Micro-Structure

Fig. 9 shows the test specimen after fracture occurred during testing along with photographs of the microstructure. As shown in Fig. (a), the CR340 and CFRP test specimens were well adhered after fracture, as was assumed in the simulation. Fig. 9(b) confirms that the porosity was minimal since CR340/CFRP composites were prepared under pressure of 0.4 MPa.[17] This result is very important because the simulation assumed that the material is a homogenous one. If the porosity is high in the CFRP, the strength would be largely impaired, and the result would not match the simulation results well.

4. Conclusions

In this study, a CR340/CFRP composite was investigated through a three-point bending test and simulations, and the experimental and simulation results were compared. To obtain accurate simulation data, a forming limit diagram was created through a stretch test for the CR340 steel plate and used as data input in the simulation. In contrast, for CFRP, the simulation data was obtained by the Hashin damage theory and damage evolution from references. The fracture mechanism in the specimen revealed a very important difference, as shown in the results. Further, accurate data input in the elastic, plastic, and fracture regions yielded similar results in the experiments and simulation. The simulation assumed that the material is a homogenous one because the porosity is very low. Thus, maximum bending stress, fracture displacement, and gradient in the experiment were almost the same as those obtained by the simulation. But the gradient error between experiment and simulation result was observed when displacement was less than 1 mm in bending test of CR340/CFRP composites. The reason for this error is explained as below.

The bending velocity was 10 mm/min in the experiment but 10mm/sec was used in simulation to reduce analysis time. When the large inertia of the punch made contact with the CR340/CFRP specimen at a high velocity in the simulation, the stress applied was grater in the simulation than the stress in the experiment. If the property of normal behavior is controlled in detailed way, more accurate result will be produced.

ACKNOWLEDGEMENT

This study was supported by a National Research Foundation of Korea (NRF) grant funded by the Korea government (MSIP) through GCRC-SOP (No. 2011-0030013).

REFERENCES

1. Jeong, Y. C., Cho, Y. T., and Jung, Y. G., “Design of Stitch Welded Shape with Laser-ARC Hybrid Welding for Ultra-High Strength Steel,” Int. J. Precis. Eng. Manuf.-Green Tech., Vol. 3, No. 2, pp. 193-197, 2016.
2. Yoon, T. H., Kim, H., Heo, C., and Kwon, J., “An Experiment and FE Simulation for the Development of a SPFC1180 AHSS One-Body Door Impact Beam about a Car Side Collision,” Int. J. Precis. Eng. Manuf., Vol. 17, No. 1, pp. 81-89, 2016.
3. Haider, A.-Z., Zhao, X.-L., and Al-Mihaidi, R., “Mechanical Behaviour of Normal Modulus Carbon Fibre Reinforced Polymer (CFRP) and Epoxy under Impact Tensile Loads,” Procedia Engineering, Vol. 10, pp. 2453-2458, 2011.

4. Choi, S.-W., Lee, M.-S., and Kang, C.-G., "Effect of Process Parameters and Laminating Methods on Spring-Back in V-Bending of CFRP/CR340 Hybrid Composites," Int. J. Precis. Eng. Manuf., Vol. 17, No. 3, pp. 395-400, 2016.

5. Jung, K.-W., Kawahito, Y., and Katayama, S., "Mechanical Property and Joining Characteristics of Laser Direct Joining of CFRP to Polyethylene Terephthalate," Int. J. Precis. Eng. Manuf.-Green Tech., Vol. 1, No. 1, pp. 43-48, 2014.

6. Teng, J., Fernando, D., Yu, T., and Zhao, X., "Debonding Failures in CFRP-Strengthened Steel Structures," Proc. of the 3rd Asia-Pacific Conference on FRP in Structures, Paper No. Key 02, 2012.

7. Narmashiri, K., Jumaat, M. Z., and Sulong, N. R., "Shear Strengthening of Steel I-Beams by Using CFRP Strips," Scientific Research and Essays, Vol. 5, No. 16, pp. 2155-2168, 2010.

8. El-Tawil, S., Ekiz, E., Goel, S., and Chao, S.-H., "Retraining Local and Global Buckling Behavior of Steel Plastic Hinges Using CFRP," Journal of Constructional Steel Research, Vol. 67, No. 3, pp. 261-269, 2011.

9. Hankeln, F. and Mahnken, R., "A Mesoscopic Model for Deep Drawing of Carbon Fibre Prepregs at Large Strains," Composite Structures, Vol. 105, pp. 340-350, 2013.

10. Cui, W., Wisnom, M., and Jones, M., "A Comparison of Failure Criteria to Predict Delamination of Unidirectional Glass/Epoxy Specimens Waisted through the Thickness," Composites, Vol. 23, No. 3, pp. 158-166, 1992.

11. Hashin, Z. and Rotem, A., "A Fatigue Failure Criterion for Fiber Reinforced Materials," Journal of Composite Materials, Vol. 7, No. 4, pp. 448-464, 1973.

12. Hashin, Z., "Failure Criteria for Unidirectional Fiber Composites," Journal of Applied Mechanics, Vol. 47, No. 2, pp. 329-334, 1980.

13. Camanho, P. P. and Dávila, C. G., "Mixed-Mode Decohesion Finite Elements for the Simulation of Delamination in Composite Materials," NASA, Report No. NASA/TM-2002-211737, L-18194, NAS 1.15:211737, 2002.

14. SIMULIA, "Abaqus User's Manual 6.9," 2010.

15. ACP Composites, "Carbon Fiber," http://www.acpsales.com/OnlineStore.php?cat=4920 (Accessed 23 September 2016)

16. Pinho, S. T., Robinson, P., and Iannucci, L., "Fracture Toughness of the Tensile and Compressive Fibre Failure Modes in Laminated Composites," Composites Science and Technology, Vol. 66, No. 13, pp. 2069-2079, 2006.

17. Zhu, H., Wu, B., Li, D., Zhang, D., and Chen, Y., "Influence of Voids on the Tensile Performance of Carbon/Epoxy Fabric Laminates," Journal of Materials Science & Technology, Vol. 27, No. 1, pp. 69-73, 2011.